Analysis and Improvement of the Consistency of Extended Kalman Filter based SLAM

Guoquan Huang, Anastasios I. Mourikis and Stergios I. Roumeliotis

Multiple Autonomous
Robotic Systems Labroratory

Technical Report
Number -2007-0001
August 2007

Dept. of Computer Science & Engineering
University of Minnesota
4-192 EE/CS Building
200 Union St. S.E.
Minneapolis, MN 55455
Tel: (612) 625-2217
Fax: (612) 625-0572
URL: http://www.cs.umn.edu/~ghuang

Analysis and Improvement of the Consistency of Extended Kalman Filter based SLAM

Guoquan Huang, Anastasios I. Mourikis and Stergios I. Roumeliotis

Multiple Autonomous Robotic Systems Laboratory, TR-2007-0001

August 2007

Abstract

In this work, we study the inconsistency of the EKF-based SLAM algorithm from the perspective of observability. We analytically prove that when the Jacobians of the state and measurement models are evaluated at the latest state estimates during every time step, the linearized error-state system model of the EKF-based SLAM has observable subspace of dimension higher than that of the actual, nonlinear, SLAM system. As a result, the covariance estimates of the EKF undergo reduction in directions of the state space where no information is available, which is a primary cause of inconsistency. Furthermore, a new "First Estimates Jacobian" (FEJ) EKF is proposed to improve the estimator's consistency during SLAM. The proposed algorithm performs better with respect to consistency, because when the filter Jacobians are calculated using the first-ever available estimates for each state variable, the error-state system model has the same observable subspace as the underlying nonlinear SLAM system. The theoretical analysis is validated through extensive simulations.

1 Introduction

Simultaneous localization and mapping (SLAM) is the process of building a map of an environment and concurrently generating an estimate of the robot pose from the sensor readings. SLAM is considered an essential capability for autonomous vehicles exploring unknown environments. Since Smith *et al.* first introduced a stochastic mapping solution to the SLAM problem [1] in the late 1980s, rapid and exciting progress in solving the problem has been made over the past decades, resulting in several competing solutions. Recent interest in SLAM has focused on the design of estimation algorithms [2, 3], data association techniques [4] and sensor data processing [5]. Among the algorithms developed thus far to solve the SLAM problem, extended Kalman filter (EKF)-based SLAM remains one of the most popular ones and has been used in many SLAM applications (e.g. [6, 7, 8]). However, in spite of its widespread adoption in practical applications, the fundamental issue of the consistency of the standard world-centric EKF-SLAM has not yet been sufficiently investigated.

As defined in [9], a state estimator is *Consistent* if the estimation errors (i) are zero-mean, and (ii) have covariance matrix smaller or equal to the one calculated by the filter. Consistency is one of the primary criteria for evaluating the performance of any estimator; if an estimator is inconsistent, then the accuracy of the produced state estimates is unknown, which in turn makes the estimator unreliable. Since SLAM is a nonlinear estimation problem, no provably consistent estimator can be constructed for it. The consistency of every estimator has to be evaluated experimentally. In particular for the *standard* EKF-SLAM algorithm, there exists significant empirical evidence showing that the computed state estimates tend to be *inconsistent.*

In this paper, we investigate in depth the fundamental cause of the inconsistency of the standard EKF-SLAM algorithm. In particular, we revisit this problem from a new perspective, i.e., by analyzing the observability properties of the filter's system model. The major contributions of this work are the following:

- Through an observability analysis, we prove that the standard EKF-SLAM employs an error-state system model that has an unobservable subspace of dimension two, even though the underlying nonlinear system model has three unobservable degrees of freedom (corresponding to the position and orientation of the global reference frame). This is a primary cause of filter inconsistency.

- We propose a new algorithm, termed *First Estimates Jacobian* (FEJ)-EKF, which improves the estimator's consistency during SLAM. Specifically, we show analytically that when the EKF state and measurement model Jacobians are computed using the first-ever available estimates for each of the state variables, the error-state model has the *same* observability properties as the underlying nonlinear model. As a result of these properties, the new FEJ-EKF outperforms, in terms of accuracy and consistency, alternative approaches to this problem [10].

The remainder of the paper is organized as follows. After an overview of related work in the next section, the observability analysis of SLAM is presented in 3, and it is employed to prove that the standard EKF-SLAM always has incorrect observability properties. Section 4 describes the proposed FEJ-EKF algorithm, and in Section 5 the performance of this new estimator is compared with that of existing solutions [10] through Monte-Carlo simulations. Finally, Section 6 outlines the main conclusions of this work.

2 Related Work

Several researchers have recently identified the inconsistency problem of the standard EKF-SLAM algorithm [10, 11, 12, 13, 14]. The first work to draw attention to this issue was that of Julier and Uhlmann [12]. Specifically, in [12] it was observed that when a stationary robot measures the relative position of a new landmark multiple times, the estimated variance of the robot's orientation becomes smaller. Since the observation of a previously unseen feature does not provide any information about the robot's state, this reduction is "artificial" and leads to inconsistency. Bailey *et al.* [11] examined several symptoms of the inconsistency of the standard EKF algorithm, and argued, based on simulation results, that the uncertainty in the robot orientation is the main cause of the inconsistency of EKF-SLAM. The work of [14] further confirmed the empirical findings in [11], and argued by example that in EKF-SLAM the inconsistency is always in the form of overconfident estimates (i.e., computed covariances smaller than the actual ones).

All the aforementioned works have described serval symptoms of the inconsistency that arises in the standard world-centric EKF-SLAM. However, they have not conducted a detailed analysis into the exact cause of the inconsistency (with the exception of [12] for the special case of a stationary robot). In this work, we study the observability properties of the standard EKF-SLAM system model, and *prove* that a mismatch in the dimensions of the observable subspace of the EKF error-state system model and the underlying nonlinear system always exists.

The observability properties of SLAM have been studied in few only cases in the literature. In particular, Andrade-Cetto *et al.* [15, 16] investigated the observability of a simple *linear time invariant* (LTI) SLAM system, and showed that it is unobservable. On the other hand, in [17] the observability of the nonlinear SLAM system was studied, using the nonlinear observability rank condition developed by Hermann and Krener [18]. This work proved that the underlying, nonlinear, SLAM system is unobservable, with three unobservable degrees of freedom. However, to the best of our knowledge, an analysis of the observability properties of the EKF linearized error-state system model does not exist to date. As shown in this paper, these properties play a significant role in determining the consistency of the filter.

3 SLAM Observability Analysis

In this section, we perform an analysis of the observability properties of the EKF linearized error-state system model. In the following, after presenting the equations of the standard EKF-SLAM formulation, we compare its observability properties with those of the underlying nonlinear system, and use this analysis to draw conclusions about the consistency of the filter. To preserve the clarity of the presentation, in this section we consider the case where a *single* landmark is included in the state vector.

3.1 Standard EKF-SLAM

In the standard formulation of SLAM the state vector comprises the robot pose and the landmarks' positions in the global frame. Thus, at time step k the state vector is given by

$$\mathbf{X}_k = \begin{bmatrix} \mathbf{p}_{R_k} \\ \phi_{R_k} \\ \mathbf{p}_L \end{bmatrix} = \begin{bmatrix} \mathbf{X}_{R_k} \\ \mathbf{p}_L \end{bmatrix} \tag{1}$$

where $\mathbf{X}_{R_k} = \begin{bmatrix} \mathbf{p}_{R_k} \\ \phi_{R_k} \end{bmatrix}$ denotes the robot pose (position and orientation), and $\mathbf{p}_L$ is the landmark position. EKF-SLAM recursively evolves in two steps: propagation and update, based on the discrete-time process and measurement models, respectively.

3.1.1 EKF Propagation

In the propagation step, the robot's odometry measurements are processed to obtain an estimate of the pose change between two consecutive time steps, and then employed in the EKF to propagate the robot state estimate. On the other hand, since the landmark is static, its state estimate does not change with the incorporation of a new odometry measurement. The EKF propagation equations are given by:[1]

$$\hat{\mathbf{p}}_{R_{k+1|k}} = \hat{\mathbf{p}}_{R_{k|k}} + \mathbf{C}(\hat{\phi}_{R_{k|k}})^{R_k}\hat{\mathbf{p}}_{R_{k+1}} \tag{2}$$

$$\hat{\phi}_{R_{k+1|k}} = \hat{\phi}_{R_{k|k}} + {}^{R_k}\hat{\phi}_{R_{k+1}} \tag{3}$$

$$\hat{\mathbf{p}}_{L_{k+1|k}} = \hat{\mathbf{p}}_{L_{k|k}} \tag{4}$$

where $\mathbf{C}(\cdot)$ denotes the 2×2 rotation matrix, and ${}^{R_k}\hat{\mathbf{X}}_{R_{k+1}} = \begin{bmatrix} {}^{R_k}\hat{\mathbf{p}}_{R_{k+1}} \\ {}^{R_k}\hat{\phi}_{R_{k+1}} \end{bmatrix}$ is the odometry-based estimate of the robot's motion between time-steps k and $k+1$. This estimate is corrupted by zero-mean, white Gaussian noise $\mathbf{w}_k = {}^{R_k}\mathbf{X}_{R_{k+1}} - {}^{R_k}\hat{\mathbf{X}}_{R_{k+1}}$, with covariance matrix $\mathbf{Q}_k$.

In addition to the state propagation equations, the linearized error-state propagation equation is necessary for the EKF. Similarly to (2)-(3), the true state propagation equations can written as follows:

$$\mathbf{p}_{R_{k+1}} = \mathbf{p}_{R_k} + \mathbf{C}(\phi_{R_k})^{R_k}\mathbf{p}_{R_{k+1}} \tag{5}$$

$$\phi_{R_{k+1}} = \phi_{R_k} + {}^{R_k}\phi_{R_{k+1}} \tag{6}$$

$$\mathbf{p}_{L_{k+1}} = \mathbf{p}_{L_k} \tag{7}$$

By subtracting (2)-(4) from (5)-(7), respectively, we have the error state propagation equations as follows:

$$\tilde{\mathbf{p}}_{R_{k+1|k}} = \tilde{\mathbf{p}}_{R_{k|k}} + \mathbf{C}(\phi_{R_k})^{R_k}\mathbf{p}_{R_{k+1}} - \mathbf{C}(\hat{\phi}_{R_{k|k}})^{R_k}\hat{\mathbf{p}}_{R_{k+1}} \tag{8}$$

$$\tilde{\phi}_{R_{k+1|k}} = \tilde{\phi}_{R_{k|k}} + {}^{R_k}\tilde{\phi}_{R_{k+1}} \tag{9}$$

$$\tilde{\mathbf{p}}_{L_{k|k+1}} = \tilde{\mathbf{p}}_{L_{k|k}} \tag{10}$$

Clearly Eq. (8) is nonlinear, we therefore linearize it at the estimated states $\hat{\phi}_{R_{k|k}}$ and ${}^{R_k}\hat{\mathbf{p}}_{R_{k+1}}$ as follows:

$$\tilde{\mathbf{p}}_{R_{k+1|k}} = \tilde{\mathbf{p}}_{R_{k|k}} + \mathbf{J}\mathbf{C}(\hat{\phi}_{R_{k|k}})^{R_k}\hat{\mathbf{p}}_{R_{k+1}}\tilde{\phi}_{R_{k|k}} + \mathbf{C}(\hat{\phi}_{R_{k|k}})^{R_k}\tilde{\mathbf{p}}_{R_{k+1}} \tag{11}$$

where $\mathbf{J} \triangleq \begin{bmatrix} 0 & -1 \\ 1 & 0 \end{bmatrix}$. By stacking the error state propagation equations (11), (9) and (10) into the block matrix form, we obtain the following familiar equation:

$$\begin{aligned} \tilde{\mathbf{X}}_{k+1|k} &= \begin{bmatrix} \mathbf{\Phi}_{R_k} & \mathbf{0}_{3\times 2} \\ \mathbf{0}_{2\times 3} & \mathbf{I}_2 \end{bmatrix} \begin{bmatrix} \tilde{\mathbf{X}}_{R_{k|k}} \\ \tilde{\mathbf{p}}_{L_{k|k}} \end{bmatrix} + \begin{bmatrix} \mathbf{G}_{R_k} \\ \mathbf{0}_{2\times 2} \end{bmatrix} \mathbf{w}_k \\ &\triangleq \mathbf{\Phi}_k \tilde{\mathbf{X}}_{k|k} + \mathbf{G}_k \mathbf{w}_k \end{aligned} \tag{12}$$

[1] Throughout this paper the subscript $\ell|j$ refers to the estimate of a quantity at time step ℓ, after all measurements up to time step j have been processed. $\hat{x}$ is used to denote the estimate of a random variable x, while $\tilde{x} = x - \hat{x}$ is the error in this estimate. $\mathbf{0}_{m\times n}$ and $\mathbf{1}_{m\times n}$ denote $m \times n$ matrices of zeros and ones, respectively, while $\mathbf{I}_n$ is the $n \times n$ identity matrix. Finally, we use the concatenated forms $s\phi$ and $c\phi$ to denote the $\sin\phi$ and $\cos\phi$ functions, respectively.

where the state transition matrices $\mathbf{\Phi}_{R_k}$ and $\mathbf{G}_{R_k}$ are given by:

$$\mathbf{\Phi}_{R_k} = \begin{bmatrix} \mathbf{I}_2 & \mathbf{J}\mathbf{C}(\hat{\phi}_{R_{k|k}})^{R_k}\hat{\mathbf{p}}_{R_{k+1}} \\ \mathbf{0}_{1\times 2} & 1 \end{bmatrix} \tag{13}$$

$$\equiv \begin{bmatrix} \mathbf{I}_2 & \mathbf{J}\left(\hat{\mathbf{p}}_{R_{k+1|k}} - \hat{\mathbf{p}}_{R_{k|k}}\right) \\ \mathbf{0}_{1\times 2} & 1 \end{bmatrix} \tag{14}$$

$$\mathbf{G}_{R_k} = \begin{bmatrix} \mathbf{C}(\hat{\phi}_{R_{k|k}}) & \mathbf{0}_{2\times 1} \\ \mathbf{0}_{1\times 2} & 1 \end{bmatrix} \tag{15}$$

It is important to point out that the form of the propagation equations presented above (cf. (2)-(3) and (12)) is general, and holds for any robot kinematic model (e.g., unicycle, bicycle, or Ackerman model). For example, if the unicycle model is used, and we employ the approximation that the velocity and heading are constant during each propagation interval, we obtain ${}^{R_k}\hat{\mathbf{X}}_{R_{k+1}} = \begin{bmatrix} v_{m_k}\delta t \\ 0 \\ \omega_{m_k}\delta t \end{bmatrix}$, where v_{m_k} and ω_{m_k} are the linear and rotational velocity measurements, respectively, and δt is the sampling period. Substitution in (2)-(3) yields the familiar robot pose propagation equations:

$$\hat{\mathbf{p}}_{R_{k+1|k}} = \hat{\mathbf{p}}_{R_{k|k}} + \begin{bmatrix} v_{m_k}\delta t c(\hat{\phi}_{R_{k|k}}) \\ v_{m_k}\delta t s(\hat{\phi}_{R_{k|k}}) \end{bmatrix} \tag{16}$$

$$\hat{\phi}_{R_{k+1|k}} = \hat{\phi}_{R_{k|k}} + \omega_{m_k}\delta t \tag{17}$$

Similarly, the commonly used expressions for the matrices $\mathbf{\Phi}_{R_k}$ and $\mathbf{G}_{R_k}$ can be derived from (13) and (15). Specifically, substitution of ${}^{R_k}\hat{\mathbf{p}}_{R_{k+1}} = \begin{bmatrix} v_{m_k}\delta t \\ 0 \end{bmatrix}$ into (13) yields:

$$\mathbf{\Phi}_{R_k} = \begin{bmatrix} \mathbf{I}_2 & \mathbf{J}\mathbf{C}(\hat{\phi}_{R_{k|k}}) \begin{bmatrix} v_{m_k}\delta t \\ 0 \end{bmatrix} \\ \mathbf{0}_{1\times 2} & 1 \end{bmatrix} = \begin{bmatrix} 1 & 0 & -v_{m_k}\delta t s(\hat{\phi}_{R_{k|k}}) \\ 0 & 1 & v_{m_k}\delta t c(\hat{\phi}_{R_{k|k}}) \\ 0 & 0 & 1 \end{bmatrix} \tag{18}$$

Because in this case the odometry provides the linear velocity v_m and rotational velocity ω_m, instead of the robot displacement ${}^{R_k}\hat{\mathbf{X}}_{R_{k+1}}$, the matrix $\mathbf{G}_{R_k}$ can be derived by using chain rule as follows:

$$\mathbf{G}_{R_k} = \frac{\partial(\mathbf{X}_{R_{k+1}})}{\partial({}^{R_k}\mathbf{X}_{R_{k+1}})}\Big|_{{}^{R_k}\hat{\mathbf{X}}_{R_{k+1}}} \times \frac{\partial({}^{R_k}\mathbf{X}_{R_{k+1}})}{\partial(\begin{bmatrix} v_k & \omega_k \end{bmatrix}^T)}\Big|_{\begin{bmatrix} v_{m_k} & \omega_{m_k} \end{bmatrix}^T} \tag{19}$$

where the first term is the Jacobian of robot propagation with respect to the displacement, evaluated at the estimate ${}^{R_k}\hat{\mathbf{X}}_{R_{k+1}}$ and essentially is the one in (15). Similarly, the second term is the Jacobian of robot displacement with respect to linear and rotational velocities, evaluated at the odometry measurements $\begin{bmatrix} v_{m_k} \\ \omega_{m_k} \end{bmatrix}$. Since ${}^{R_k}\mathbf{X}_{R_{k+1}} = \begin{bmatrix} v_k\delta t \\ 0 \\ \omega_k\delta t \end{bmatrix}$, this Jacobian is simply given by:

$$\frac{\partial({}^{R_k}\mathbf{X}_{R_{k+1}})}{\partial(\begin{bmatrix} v_k & \omega_k \end{bmatrix}^T)}\Big|_{\begin{bmatrix} v_{m_k} & \omega_{m_k} \end{bmatrix}^T} = \begin{bmatrix} \delta t & 0 \\ 0 & 0 \\ 0 & \delta t \end{bmatrix} \tag{20}$$

Therefore, substituting the above equation (20) and (15) into (19), we obtain:

$$\mathbf{G}_{R_k} = \begin{bmatrix} \mathbf{C}(\hat{\phi}_{R_{k|k}}) & \mathbf{0}_{2\times 1} \\ \mathbf{0}_{1\times 2} & 1 \end{bmatrix} \begin{bmatrix} \delta t & 0 \\ 0 & 0 \\ 0 & \delta t \end{bmatrix} = \begin{bmatrix} \delta t c(\hat{\phi}_{R_{k|k}}) & 0 \\ \delta t s(\hat{\phi}_{R_{k|k}}) & 0 \\ 0 & \delta t \end{bmatrix} \tag{21}$$

3.1.2 EKF Update

The measurement used for updates in the EKF is a function of the relative position of the landmark with respect to the robot:

$$\mathbf{z}_k = \mathbf{h}(\mathbf{X}_k) + \mathbf{v}_k = \mathbf{h}\left(\mathbf{C}^T(\phi_{R_k})(\mathbf{p}_{L_k} - \mathbf{p}_{R_k})\right) + \mathbf{v}_k \tag{22}$$

where $\mathbf{v}_k$ is zero-mean Gaussian measurement noise with covariance $\mathbf{R}_k$. In this work, we allow $\mathbf{h}$ to be *any* 2-dimensional measurement function, as long as it is invertible (i.e., as long as we can fully determine an estimate of the robot-relative landmark position from $\mathbf{z}_k$). For instance, this is the case when $\mathbf{z}_k$ is a direct measurement of relative position, a pair of range and bearing measurements, two bearing measurements from the cameras of a stereo pair, etc. Generally, the measurement function is nonlinear, and hence it is linearized for use in the EKF. The linearized measurement error equation is given by

$$\begin{aligned}\tilde{\mathbf{z}}_k &\simeq \begin{bmatrix}\mathbf{H}_{R_k} & \mathbf{H}_{L_k}\end{bmatrix}\begin{bmatrix}\tilde{\mathbf{X}}_{R_{k|k-1}} \\ \tilde{\mathbf{X}}_{L_{k|k-1}}\end{bmatrix} + \mathbf{v}_k \\ &\triangleq \mathbf{H}_k\tilde{\mathbf{X}}_{k|k-1} + \mathbf{v}_k \end{aligned} \tag{23}$$

where $\mathbf{H}_{R_k}$ and $\mathbf{H}_{L_k}$ are the Jacobians of $\mathbf{h}$ with respect to the robot pose and the landmark position, respectively, evaluated at the state estimate $\hat{\mathbf{X}}_{k|k-1}$. Using the chain rule of derivation, these are computed as:

$$\mathbf{H}_{R_k} = (\nabla\mathbf{h}_k)\mathbf{C}^T(\hat{\phi}_{R_{k|k-1}})\begin{bmatrix}-\mathbf{I}_2 & -\mathbf{J}(\hat{\mathbf{p}}_{L_{k|k-1}} - \hat{\mathbf{p}}_{R_{k|k-1}})\end{bmatrix} \tag{24}$$

$$\mathbf{H}_{L_k} = (\nabla\mathbf{h}_k)\mathbf{C}^T(\hat{\phi}_{R_{k|k-1}}) \tag{25}$$

where $\nabla\mathbf{h}_k$ denotes the Jacobian of $\mathbf{h}$ with respect to the robot-relative landmark position (i.e., with respect to the vector ${}^{R_k}\mathbf{p}_L = \mathbf{C}^T(\phi_{R_k})(\mathbf{p}_L - \mathbf{p}_{R_k})$), evaluated at the state estimate $\hat{\mathbf{X}}_{k|k-1}$.

3.2 Observability Analysis for SLAM

Before studying the observability properties of the EKF system model, we conduct the observability analysis for the underlying continuous-time nonlinear SLAM system. By comparing the properties of the actual, nonlinear, system with those of the EKF system model, we will be able to identify a fundamental shortcoming of the standard EKF formulation, which leads to filter inconsistency. The nonlinear observability analysis is based on the *observability rank condition* introduced in [18]. Specifically, Theorem 3.11 in [18] proves that "*if a nonlinear system is locally weakly observable, the observability rank condition is satisfied generically*". We here show that the SLAM system does not satisfy the observability rank condition, and thus it is not locally weakly observable nor locally observable.

For the continuous-time analysis we employ a unicycle kinematic model, and a relative-position measurement model, although identical conclusions can be reached if different models are used [17]. In 2D SLAM the process model of the robot pose in continuous-time form is given by

$$\dot{x}_R(t) = v(t)c(\phi_R(t)) \tag{26}$$

$$\dot{y}_R(t) = v(t)s(\phi_R(t)) \tag{27}$$

$$\dot{\phi}_R(t) = \omega(t) \tag{28}$$

where $\mathbf{u} \triangleq \begin{bmatrix}v & \omega\end{bmatrix}^T$ is the control input, consisting of linear velocity and rotational velocity, respectively. The dynamics of the static landmark simply are:

$$\dot{x}_L(t) = 0 \tag{29}$$

$$\dot{y}_L(t) = 0 \tag{30}$$

In order to apply the nonlinear observability analysis using Lie derivatives, we transform the process model (cf. (26)-(28) and (29)-(30)) into input-affine function form as follows:

$$\begin{aligned}\begin{bmatrix}\dot{x}_R(t)\\ \dot{y}_R(t)\\ \dot{\phi}_R(t)\\ \dot{x}_L(t)\\ \dot{y}_L(t)\end{bmatrix} &= \begin{bmatrix}c(\phi_R(t))\\ s(\phi_R(t))\\ 0\\ 0\\ 0\end{bmatrix} v(t) + \begin{bmatrix}0\\0\\1\\0\\0\end{bmatrix}\omega(t)\\ \Rightarrow\dot{\mathbf{X}}(t) &= \mathbf{f}_1 v(t) + \mathbf{f}_2\omega(t)\end{aligned} \tag{31}$$

where $\mathbf{X} \triangleq \begin{bmatrix}x_R & y_R & \phi_R & x_L & y_L\end{bmatrix}^T$ is the state vector of the system. We here consider the case where the robot-to-landmark measurements are relative-position measurements, which is the most common type of measurements used for 2D SLAM (such measurements are, for example, provided when corner features are detected in laser scans). The relative position measurement can be written in continuous-time form as follows:

$$\begin{aligned}\mathbf{z}(t) = \mathbf{C}^T(\phi_R(t))(\mathbf{p}_L(t) - \mathbf{p}_R(t)) &= \begin{bmatrix} c(\phi_R(t))(x_L(t) - x_R(t)) + s(\phi_R(t))(y_L(t) - y_R(t))\\ -s(\phi_R(t))(x_L(t) - x_R(t)) + c(\phi_R(t))(y_L(t) - y_R(t))\end{bmatrix}\\ \Rightarrow\mathbf{z}(t) &= \begin{bmatrix}h_1(\mathbf{X})\\ h_2(\mathbf{X})\end{bmatrix}\end{aligned} \tag{32}$$

Now we are able to find the observability matrix by computing the Lie derivatives of the nonlinear system defined in (31) and (32). We define the Lie derivative of a C^∞ function h on an open subset $\mathcal{S} \subset \mathbb{R}^{dim(\mathbf{X})}$ along an analytic vector field $\mathbf{f}$ on $\mathcal{S}$, as:

$$L_{\mathbf{f}} h = (dh)^T\mathbf{f} \tag{33}$$

where dh is the gradient of h. Applying this definition to the SLAM system, note that $\mathbf{f}_1$ and $\mathbf{f}_2$ are a vector field on $\mathcal{S}$ and we can calculate the Lie derivatives of h_1 and h_2 along them. First the gradients of h_1 and h_2 (or zeroth-order Lie derivatives) are computed as follows (the time index t will henceforth be dropped to simplify the notation):

$$dh_1^T = \begin{bmatrix}-c(\phi_R) & -s(\phi_R) & -s(\phi_R)(x_L - x_R) + c(\phi_R)(y_L - y_R) & c(\phi_R) & s(\phi_R)\end{bmatrix} \tag{34}$$

$$dh_2^T = \begin{bmatrix}s(\phi_R) & -c(\phi_R) & -c(\phi_R)(x_L - x_R) - s(\phi_R)(y_L - y_R) & -s(\phi_R) & c(\phi_R)\end{bmatrix} \tag{35}$$

The first-order Lie derivatives are calculated according to the definition (33).

$$L_{\mathbf{f_1}} h_1 = -1 \tag{36}$$

$$L_{\mathbf{f_1}} h_2 = 0 \tag{37}$$

$$L_{\mathbf{f_2}} h_1 = -s(\phi_R)(x_L - x_R) + c(\phi_R)(y_L - y_R) \tag{38}$$

$$L_{\mathbf{f_2}} h_2 = -c(\phi_R)(x_L - x_R) - s(\phi_R)(y_L - y_R) \tag{39}$$

Because $L_{\mathbf{f_1}} h_1$ and $L_{\mathbf{f_1}} h_2$ are constant, their gradients are equal to zero. Therefore, we only need to consider $L_{\mathbf{f_2}} h_1$ and $L_{\mathbf{f_2}} h_2$, in computing the second-order Lie derivatives. We obtain:

$$L_{f_1}(L_{f_2} h_1) = 0 \tag{40}$$

$$L_{f_2}(L_{f_2} h_1) = -c(\phi_R)(x_L - x_R) - s(\phi_R)(y_L - y_R) \tag{41}$$

$$L_{f_1}(L_{f_2} h_2) = 1 \tag{42}$$

$$L_{f_2}(L_{f_2} h_2) = s(\phi_R)(x_L - x_R) - \cos(\phi_R)(y_L - y_R) \tag{43}$$

Clearly, the second-order Lie derivatives are linear combination of the first-order ones. If we compute the higher-order Lie derivatives, it is not difficult to realize that the higher-order Lie derivatives depend linearly on the first-order ones. Therefore, the space spanned by all the kth order Lie derivatives $L^k_{\mathbf{f}_j} h_i (\forall k \in \mathbb{R}^1, j =$

$1, 2, i = 1, 2)$ which will be denoted by $\mathcal{G}$, is equivalent to the space spanned by only the first-order Lie derivatives, i.e.,

$$\mathcal{G} = span\{L_{\mathbf{f_1}}h_1, L_{\mathbf{f_1}}h_2, L_{\mathbf{f_2}}h_1, L_{\mathbf{f_2}}h_2\} \tag{44}$$

Consequently, the space $d\mathcal{G}$ spanned by the gradients of the elements of $\mathcal{G}$ is given by

$$\begin{aligned} d\mathcal{G} =& span\{dL_{\mathbf{f_1}}h_1, dL_{\mathbf{f_1}}h_2, dL_{\mathbf{f_2}}h_1, dL_{\mathbf{f_2}}h_2\} \\ =& span \begin{bmatrix} s(\phi_R) & -c(\phi_R) & -c(\phi_R)(x_L - x_R) - s(\phi_R)(y_L - y_R) & -s(\phi_R) & c(\phi_R) \\ c(\phi_R) & s(\phi_R) & s(\phi_R)(x_L - x_R) - c(\phi_R)(y_L - y_R) & -c(\phi_R) & -s(\phi_R) \end{bmatrix} \end{aligned} \tag{45}$$

where the rows that equal to zero have been omitted. The matrix shown above is the "observability matrix" for the nonlinear SLAM system under consideration. Clearly, the rank of this matrix is two, and thus the system is unobservable. Intuitively, this is a consequence of the fact that we cannot gain *absolute*, but rather only *relative* state information from the available measurements.

Even though the notion of an "unobservable subspace" cannot be strictly defined for this system, by examining the physical interpretation of the basis of $d\mathcal{G}^{\perp}$, we will gain useful information for our analysis in Section 3.2.1. By inspection, we see that one possible basis for the space $d\mathcal{G}^{\perp}$ is given by

$$d\mathcal{G}^{\perp} = \text{span} \begin{bmatrix} 1 & 0 & -y_R \\ 0 & 1 & x_R \\ 0 & 0 & 1 \\ 1 & 0 & -y_L \\ 0 & 1 & x_L \end{bmatrix} \triangleq \text{span} \begin{bmatrix} \mathbf{n}_1 & \mathbf{n}_2 & \mathbf{n}_3 \end{bmatrix} \tag{46}$$

From the structure of the vectors $\mathbf{n}_1$ and $\mathbf{n}_2$ we see that a change in the state by $\Delta\mathbf{X} = \alpha\mathbf{n}_1 + \beta\mathbf{n}_2$, $\alpha, \beta \in \mathbb{R}$ corresponds to a "shifting" of the $x - y$ plane by α units along x, and by β units along y. Thus, if the robot and landmark positions are shifted equally, the states $\mathbf{X}$ and $\mathbf{X} + \Delta\mathbf{X}$ will be indistinguishable given the measurements. To better understand the physical meaning of $\mathbf{n}_3$, we consider the case where the $x - y$ plane is rotated by a small angle $\delta\phi$. Rotating the coordinate system transforms any point $\mathbf{x} = [x \;\; y]^T$ to a point $\mathbf{x}' = [x' \;\; y']^T$, given by:

$$\begin{bmatrix} x' \\ y' \end{bmatrix} = \mathbf{C}(\delta\phi) \begin{bmatrix} x \\ y \end{bmatrix} \simeq \begin{bmatrix} 1 & -\delta\phi \\ \delta\phi & 1 \end{bmatrix} \begin{bmatrix} x \\ y \end{bmatrix} = \begin{bmatrix} x \\ y \end{bmatrix} + \delta\phi \begin{bmatrix} -y \\ x \end{bmatrix}$$

where we have employed the small angle approximations $c(\delta\phi) \simeq 1$ and $s(\delta\phi) \simeq \delta\phi$. Using this result, we see that if the plane containing the robot and landmarks is rotated by $\delta\phi$, the SLAM state vector will change to

$$\mathbf{X}' = \begin{bmatrix} x'_R \\ y'_R \\ \phi'_R \\ x'_L \\ x'_L \end{bmatrix} \simeq \begin{bmatrix} x_R \\ y_R \\ \phi_R \\ x_L \\ x_L \end{bmatrix} + \delta\phi \begin{bmatrix} -y_R \\ x_R \\ 1 \\ -y_L \\ x_L \end{bmatrix} = \mathbf{X} + \delta\phi\mathbf{n}_3 \tag{47}$$

which indicates that the vector $\mathbf{n}_3$ corresponds to a rotation of the $x - y$ plane. Since $\mathbf{n}_3 \in d\mathcal{G}^{\perp}$, this result shows that any such rotation is unobservable, and will cause no change to the measurements. The preceding analysis for the meaning of the basis vectors of $d\mathcal{G}^{\perp}$ agrees with intuition, which dictates that the *global coordinates* of the state vector in SLAM (rotation and translation) are unobservable.

3.2.1 EKF-SLAM Observability Analysis

In the previous section it was shown that the underlying physical system in SLAM has three unobservable degrees of freedom. Thus, when the EKF is used for state estimation in SLAM, we would expect that the system model employed by the EKF also shares this property. However, in this section we show that this is not the case, since the unobservable subspace of the linearized error-state model of the standard EKF is generally of dimension only 2.

Since the linearized error-state model for EKF-SLAM is time-varying, we employ the *local observability matrix* [19] to perform the observability analysis. Specifically, for the EKF-SLAM system considered in this work (cf. (12) and (23)), the local observability matrix for the time interval between time-steps k and $k+m$ is defined as:

$$\mathbf{M} \triangleq \begin{bmatrix} \mathbf{H}_k \\ \mathbf{H}_{k+1}\mathbf{\Phi}_k \\ \vdots \\ \mathbf{H}_{k+m}\mathbf{\Phi}_{k+m-1}\cdots\mathbf{\Phi}_k \end{bmatrix} \tag{48}$$

which can be expanded by substituting the matrices $\mathbf{\Phi}_i$ and $\mathbf{H}_i$ (cf. (12) and (23), respectively), to yield:

$$\mathbf{M} = \begin{bmatrix} \mathbf{H}_{R_k} & \mathbf{H}_{L_k} \\ \mathbf{H}_{R_{k+1}}\mathbf{\Phi}_{R_k} & \mathbf{H}_{L_{k+1}} \\ \vdots & \vdots \\ \mathbf{H}_{R_{k+m}}\mathbf{\Phi}_{R_{k+m-1}}\cdots\mathbf{\Phi}_{R_k} & \mathbf{H}_{L_{k+m}} \end{bmatrix} \tag{49}$$

$$=\mathbf{Diag}(\mathbf{H}_{L_k},\cdots,\mathbf{H}_{L_{k+m}}) \times \underbrace{\begin{bmatrix} \mathbf{H}_{L_k}^{-1}\mathbf{H}_{R_k} & \mathbf{I}_2 \\ \mathbf{H}_{L_{k+1}}^{-1}\mathbf{H}_{R_{k+1}}\mathbf{\Phi}_{R_k} & \mathbf{I}_2 \\ \vdots & \vdots \\ \mathbf{H}_{L_{k+m}}^{-1}\mathbf{H}_{R_{k+m}}\mathbf{\Phi}_{R_{k+m-1}}\cdots\mathbf{\Phi}_{R_k} & \mathbf{I}_2 \end{bmatrix}}_{\mathbf{N}} \tag{50}$$

where $\mathbf{Diag}(\cdot)$ denotes the block-diagonal matrix. The system is locally observable over the time period from k to $k+m$ if and only if the local observability matrix $\mathbf{M}$ is full-rank. Since the matrix $\mathbf{Diag}(\mathbf{H}_{L_k},\cdots,\mathbf{H}_{L_{k+m}})$ is nonsingular, it becomes clear that rank($\mathbf{M}$) = rank($\mathbf{N}$), and moreover, the matrices $\mathbf{M}$ and $\mathbf{N}$ have the same right nullspace. Therefore, studying the rank and nullspace of $\mathbf{N}$ is equivalent to studying those of $\mathbf{M}$.

3.2.2 Ideal EKF-SLAM

Before considering the rank of the matrix $\mathbf{M}$, which is constructed using the *estimated* values of the state in the filter Jacobians, it is interesting to study the observability properties of the "oracle", or "ideal" EKF (i.e., the filter whose Jacobians are evaluated using the *true* values of the state variables). In the following, all matrices evaluated using the true state values are denoted by the symbol " ˘ ".

We start by noting that (cf. (14)):

$$\breve{\mathbf{\Phi}}_{R_{k+1}}\breve{\mathbf{\Phi}}_{R_k} = \begin{bmatrix} \mathbf{I}_2 & \mathbf{J}\left(\mathbf{p}_{R_{k+2}} - \mathbf{p}_{R_{k+1}}\right) \\ \mathbf{0}_{1\times 2} & 1 \end{bmatrix} \begin{bmatrix} \mathbf{I}_2 & \mathbf{J}\left(\mathbf{p}_{R_{k+1}} - \mathbf{p}_{R_k}\right) \\ \mathbf{0}_{1\times 2} & 1 \end{bmatrix} = \begin{bmatrix} \mathbf{I}_2 & \mathbf{J}\left(\mathbf{p}_{R_{k+2}} - \mathbf{p}_{R_k}\right) \\ \mathbf{0}_{1\times 2} & 1 \end{bmatrix} \tag{51}$$

Based on this property, it is easy to show by induction that:

$$\breve{\mathbf{\Phi}}_{R_{k+i-1}}\breve{\mathbf{\Phi}}_{R_{k+i-2}}\cdots\breve{\mathbf{\Phi}}_{R_k} = \begin{bmatrix} \mathbf{I}_2 & \mathbf{J}\left(\mathbf{p}_{R_{k+i}} - \mathbf{p}_{R_k}\right) \\ \mathbf{0}_{1\times 2} & 1 \end{bmatrix} \tag{52}$$

which holds for all $i > 0$. Using this result, and substituting for the measurement Jacobians from (24) and (25), we can prove the following useful identity:

$$\begin{aligned}
&\breve{\mathbf{H}}_{L_{k+i}}^{-1}\breve{\mathbf{H}}_{R_{k+i}}\breve{\mathbf{\Phi}}_{R_{k+i-1}}\cdots\breve{\mathbf{\Phi}}_{R_k}\\
=&\mathbf{C}^{-T}(\phi_{R_{k+i}})(\nabla\breve{\mathbf{h}}_{k+i})^{-1}\left((\nabla\breve{\mathbf{h}}_{k+i})\mathbf{C}^T(\phi_{R_{k+i}})\begin{bmatrix}-\mathbf{I}_2 & -\mathbf{J}(\mathbf{p}_L-\mathbf{p}_{R_{k+i}})\end{bmatrix}\right)\begin{bmatrix}\mathbf{I}_2 & \mathbf{J}\left(\mathbf{p}_{R_{k+i}}-\mathbf{p}_{R_k}\right)\\ \mathbf{0}_{1\times 2} & \mathbf{1}\end{bmatrix}\\
=&\mathbf{C}(\phi_{R_{k+i}})\left(-\mathbf{C}^T(\phi_{R_{k+i}})\begin{bmatrix}\mathbf{I}_2 & \mathbf{J}(\mathbf{p}_L-\mathbf{p}_{R_k})\end{bmatrix}\right)\\
=&-\begin{bmatrix}\mathbf{I}_2 & \mathbf{J}(\mathbf{p}_L-\mathbf{p}_{R_k})\end{bmatrix}\\
=&\mathbf{C}(\phi_{R_k})\left(-\mathbf{C}^T(\phi_{R_k})\begin{bmatrix}\mathbf{I}_2 & \mathbf{J}(\mathbf{p}_L-\mathbf{p}_{R_k})\end{bmatrix}\right)\\
=&\mathbf{C}^{-T}(\phi_{R_k})(\nabla\breve{\mathbf{h}}_k)^{-1}\left((\nabla\breve{\mathbf{h}}_k)\mathbf{C}^T(\phi_{R_k})\begin{bmatrix}-\mathbf{I}_2 & -\mathbf{J}(\mathbf{p}_L-\mathbf{p}_{R_k})\end{bmatrix}\right)\\
\triangleq&\breve{\mathbf{H}}_{L_k}^{-1}\breve{\mathbf{H}}_{R_k} \qquad (53)
\end{aligned}$$

which holds for all $i > 0$. The matrix $\breve{\mathbf{N}}$ can now be written as

$$\breve{\mathbf{N}}=\begin{bmatrix}\breve{\mathbf{H}}_{L_k}^{-1}\breve{\mathbf{H}}_{R_k} & \mathbf{I}_2\\ \breve{\mathbf{H}}_{L_k}^{-1}\breve{\mathbf{H}}_{R_k} & \mathbf{I}_2\\ \vdots & \vdots\\ \breve{\mathbf{H}}_{L_k}^{-1}\breve{\mathbf{H}}_{R_k} & \mathbf{I}_2\end{bmatrix}=\begin{bmatrix}-\mathbf{I}_2 & -\mathbf{J}(\mathbf{p}_L-\mathbf{p}_{R_k}) & \mathbf{I}_2\\ -\mathbf{I}_2 & -\mathbf{J}(\mathbf{p}_L-\mathbf{p}_{R_k}) & \mathbf{I}_2\\ \vdots & \vdots & \\ -\mathbf{I}_2 & -\mathbf{J}(\mathbf{p}_L-\mathbf{p}_{R_k}) & \mathbf{I}_2\end{bmatrix} \qquad (54)$$

Clearly, rank($\breve{\mathbf{N}}$) = 2 and thus the ideal EKF system model is unobservable. Most importantly, however, it can be easily verified that a basis for the right nullspace of $\breve{\mathbf{N}}$ (and thus for the right nullspace of $\breve{\mathbf{M}}$) is given by the vectors shown in (46). Thus, the unobservable subspace of the ideal EKF system model is *identical* to the space $d\mathcal{G}^{\perp}$, that contains the unobservable directions of the nonlinear SLAM system. We therefore see that if it was possible to evaluate the Jacobians using the true state values, the linearized error-state model employed in the EKF would have observability properties similar to those of the actual, nonlinear SLAM system.

3.2.3 Standard EKF-SLAM

We now study the observability properties of the standard EKF-SLAM, in which the Jacobians are evaluated at the estimated state. We start by deriving an expression similar to that of (51), for this case:

$$\begin{aligned}
\mathbf{\Phi}_{R_{k+1}}\mathbf{\Phi}_{R_k}&=\begin{bmatrix}\mathbf{I}_2 & \mathbf{J}\left(\hat{\mathbf{p}}_{R_{k+2|k+1}}-\hat{\mathbf{p}}_{R_{k+1|k+1}}\right)\\ \mathbf{0}_{1\times 2} & 1\end{bmatrix}\begin{bmatrix}\mathbf{I}_2 & \mathbf{J}\left(\hat{\mathbf{p}}_{R_{k+1|k}}-\hat{\mathbf{p}}_{R_{k|k}}\right)\\ \mathbf{0}_{1\times 2} & 1\end{bmatrix} &(55)\\
&=\begin{bmatrix}\mathbf{I}_2 & \mathbf{J}\left(\hat{\mathbf{p}}_{R_{k+2|k+1}}-\hat{\mathbf{p}}_{R_{k|k}}+\left(\hat{\mathbf{p}}_{R_{k+1|k}}-\hat{\mathbf{p}}_{R_{k+1|k+1}}\right)\right)\\ \mathbf{0}_{1\times 2} & 1\end{bmatrix} &(56)
\end{aligned}$$

Moreover, using induction, we can show that:

$$\mathbf{\Phi}_{R_{k+i-1}}\mathbf{\Phi}_{R_{k+i-2}}\cdots\mathbf{\Phi}_{R_k}=\begin{bmatrix}\mathbf{I}_2 & \mathbf{J}\left(\hat{\mathbf{p}}_{R_{k+i|k+i-1}}-\hat{\mathbf{p}}_{R_{k|k}}+\sum_{j=k}^{k+i-2}\left(\hat{\mathbf{p}}_{R_{j+1|j}}-\hat{\mathbf{p}}_{R_{j+1|j+1}}\right)\right)\\ \mathbf{0}_{1\times 2} & 1\end{bmatrix} \qquad (57)$$

which holds for all $i > 0$. And therefore:

$$\begin{aligned}
&\mathbf{H}_{L_{k+i}}^{-1}\mathbf{H}_{R_{k+i}}\mathbf{\Phi}_{R_{k+i-1}}\cdots\mathbf{\Phi}_{R_k} &(58)\\
&=-\mathbf{C}^{-T}(\phi_{R_{k+i|k+i-1}})(\nabla\mathbf{h}_{k+i})^{-1}(\nabla\mathbf{h}_{k+i})\mathbf{C}^T(\phi_{R_{k+i|k+i-1}})\begin{bmatrix}\mathbf{I}_2 & \mathbf{J}(\mathbf{p}_{L_{k+i|k+i-1}}-\mathbf{p}_{R_{k+i|k+i-1}})\end{bmatrix}\times\\
&\qquad\begin{bmatrix}\mathbf{I}_2 & \mathbf{J}\left(\hat{\mathbf{p}}_{R_{k+i|k+i-1}}-\hat{\mathbf{p}}_{R_{k|k}}+\sum_{j=k}^{k+i-2}\left(\hat{\mathbf{p}}_{R_{j+1|j}}-\hat{\mathbf{p}}_{R_{j+1|j+1}}\right)\right)\\ \mathbf{0}_{1\times 2} & 1\end{bmatrix} &(59)\\
&=-\begin{bmatrix}\mathbf{I}_2 & \mathbf{J}\left(\mathbf{p}_{L_{k+i|k+i-1}}-\hat{\mathbf{p}}_{R_{k|k}}+\sum_{j=k}^{k+i-2}\left(\hat{\mathbf{p}}_{R_{j+1|j}}-\hat{\mathbf{p}}_{R_{j+1|j+1}}\right)\right)\end{bmatrix} &(60)
\end{aligned}$$

Using this result, we can write matrix $\mathbf{N}$ as:

$$\mathbf{N} = \begin{bmatrix} -\mathbf{I}_2 & -\mathbf{J}\left(\hat{\mathbf{p}}_{L_{k|k-1}} - \hat{\mathbf{p}}_{R_{k|k-1}}\right) & \mathbf{I}_2 \\ -\mathbf{I}_2 & -\mathbf{J}\left(\hat{\mathbf{p}}_{L_{k+1|k}} - \hat{\mathbf{p}}_{R_{k|k}}\right) & \mathbf{I}_2 \\ -\mathbf{I}_2 & -\mathbf{J}\left(\hat{\mathbf{p}}_{L_{k+2|k+1}} - \hat{\mathbf{p}}_{R_{k|k}} + \left(\hat{\mathbf{p}}_{R_{k+1|k}} - \hat{\mathbf{p}}_{R_{k+1|k+1}}\right)\right) & \mathbf{I}_2 \\ \vdots & \vdots & \vdots \\ -\mathbf{I}_2 & -\mathbf{J}\left(\mathbf{p}_{L_{k+i|k+i-1}} - \hat{\mathbf{p}}_{R_{k|k}} + \sum_{j=k}^{k+i-2}\left(\hat{\mathbf{p}}_{R_{j+1|j}} - \hat{\mathbf{p}}_{R_{j+1|j+1}}\right)\right) & \mathbf{I}_2 \end{bmatrix} \tag{61}$$

At this point, we note that the estimates of any given state variable at different time instants are generally different. Therefore, the following inequalities generally hold:

$$\hat{\mathbf{p}}_{L_{k|k-1}} \neq \hat{\mathbf{p}}_{L_{k+1|k}} \neq \cdots \neq \mathbf{p}_{L_{k+i|k+i-1}} \tag{62}$$

and

$$\hat{\mathbf{p}}_{R_{k+1|k}} - \hat{\mathbf{p}}_{R_{k+1|k+1}} \neq \mathbf{0}_{2\times 1} \tag{63}$$

Therefore, the third column of $\mathbf{N}$ will be, in general, a vector with unequal elements, and hence rank($\mathbf{N}$) = 3. We thus see that the linearized error-state model employed in the standard EKF-SLAM has different observability properties than the underlying nonlinear system. In particular, by processing the measurements collected in the interval $[k, k+m]$, the EKF acquires information in 3 dimensions of the state space (along the directions corresponding to the observable subspace of the EKF). However, as the nonlinear observability analysis of Section 3.2 shows, the measurements actually provide information in only 2 directions of the state space. As a result, the EKF gains “spurious information” along the unobservable directions of the underlying nonlinear SLAM system, which leads to inconsistency.

To probe further, we note that the basis of the right nullspace of $\mathbf{N}$ is given by:

$$\text{null}(\mathbf{N}) = \begin{bmatrix} 1 & 0 \\ 0 & 1 \\ 0 & 0 \\ 1 & 0 \\ 0 & 1 \end{bmatrix} = \begin{bmatrix} \mathbf{n}_1 & \mathbf{n}_2 \end{bmatrix} \tag{64}$$

which, as explained in Section 3.2 corresponds to a shifting of the $x-y$ plane. It is interesting to point out that the “missing” direction in the unobservable subspace of the EKF system model is the one along the vector $\mathbf{n}_3$, which corresponds to a rotation of the $x-y$ plane. Therefore, we see that the filter will gain “nonexistent” information about the robot’s orientation. This will lead to an unjustified reduction in the uncertainty of the robot’s orientation, which will, in turn, further reduce the uncertainty in all the state variables. This agrees in some respects with [11, 14], where it was argued that the orientation uncertainty is the cause of the filter’s inconsistency. However, we point out that the *root cause* of the problem is the fact that the Jacobians are evaluated at different linearization points at every time step. This changes the dimension of the observable subspace, and thus fundamentally alters the properties of the estimation process.

An additional interesting point is that the covariance matrix of the measurements does not appear in the observability analysis of the filter. Therefore, even if this covariance matrix is artificially inflated, the filter will retain the same observability properties (i.e., the same observable and unobservable subspaces). This shows that no amount of covariance inflation can result in correct observability properties. Similarly, even if the Iterated EKF is employed for state estimation, the same, erroneous, observability properties will arise, since the landmark position estimates will generally differ at different time steps.

As a final remark, we note the “correct” observability properties of the ideal EKF are attributed to the fact that (53) holds, which is not the case for the standard EKF. When condition (53) is met, it ensures that all the block rows of the matrix $\mathbf{N}$ are identical, and leads to an unobservable subspace of dimension three. Thus, (53) can be seen as a sufficient condition that, when satisfied by the filter Jacobians, ensures correct observability properties.

3.2.4 Special Case - Stationary Robot

It is interesting to examine the special case where the robot remains static, while observing one landmark L at every time step. As an intuitive example to show the inconsistency of EKF-SLAM, this special case has been extensively studied in the literature [11, 14, 12]. In [12], based on the fundamental observation that the stationary robot should have zero Kalman gain for its pose, a constraint was derived for the filter Jacobians (cf. Theorem 1 therein) as follows:

$$\nabla \mathbf{h}_1^x - \nabla \mathbf{h}_1^p \nabla \mathbf{g}_1^x = \mathbf{0} \tag{65}$$

where $\nabla \mathbf{h}^x$ and $\nabla \mathbf{h}^p$ are the measurement matrices with respect to robot pose and landmark position, respectively, which are identical to $\mathbf{H}_R$ and $-\mathbf{H}_L$ in our notation, respectively. $\nabla \mathbf{g}^x$ is the landmark initialization Jacobian with respect to robot pose. In order to derive an expression for $\nabla \mathbf{g}^x$ using our notation, we note that

$$\mathbf{g}(\mathbf{X}_{R_k}, \mathbf{z}_k) = \mathbf{C}(\phi_{R_k})\mathbf{h}^{-1}(\mathbf{z}_k) + \mathbf{p}_{R_k} \tag{66}$$

where

$$\mathbf{h}^{-1}(\mathbf{z}_k) = \left(\mathbf{C}^T(\phi_{R_k})(\mathbf{p}_{L_k} - \mathbf{p}_{R_k})\right) \tag{67}$$

Therefore,

$$\nabla \mathbf{g}^x = \begin{bmatrix}\mathbf{I}_2 & \mathbf{J}\mathbf{C}(\phi_R)\mathbf{h}^{-1}(\mathbf{z}_k)\end{bmatrix} = \begin{bmatrix}\mathbf{I}_2 & \mathbf{J}(\mathbf{p}_L - \mathbf{p}_{R_k})\end{bmatrix} \tag{68}$$

Substitution in (65) yields:

$$\breve{\mathbf{H}}_{R_k} + \breve{\mathbf{H}}_{L_k} \nabla \mathbf{g}^x = \mathbf{0} \tag{69}$$

which holds for all time steps. We point out that this condition is identical to the one (53), for the special case where the robot is stationary. Specifically, we start by noting that the identity (69) is equivalent to

$$\breve{\mathbf{H}}_{L_{k+i}}^{-1} \breve{\mathbf{H}}_{R_{k+i}} = \breve{\mathbf{H}}_{L_k}^{-1} \breve{\mathbf{H}}_{R_k} \qquad i = 1, 2, \ldots \tag{70}$$

When the robot is static, the propagation stage of the EKF is trivial, and can be omitted. This is equivalent to setting $\breve{\mathbf{\Phi}}_{R_k} = \mathbf{I}_3$ for all k. In that case, Eq. (53) becomes identical to (70), which shows that the condition derived based on the observability criterion is more general and encompasses (70) as a special case.

4 First-Estimates Jacobian EKF SLAM

Careful observation of the matrix $\mathbf{N}$ in (61) reveals that it is possible to obtain an EKF system model with an unobservable subspace of dimension three, even if the Jacobians are not evaluated at the true state values. For this purpose, the following two changes are necessary.

1. Instead of computing the state-propagation Jacobian matrix $\mathbf{\Phi}_{R_k}$ as in (14), we employ the expression:

$$\mathbf{\Phi}'_{R_k} = \begin{bmatrix}\mathbf{I}_2 & \mathbf{J}\left(\hat{\mathbf{p}}_{R_{k+1|k}} - \hat{\mathbf{p}}_{R_{k|k-1}}\right) \\ \mathbf{0}_{1\times 2} & 1\end{bmatrix} \tag{71}$$

   The difference compared to (14) is that the robot position estimate prior to updating, $\hat{\mathbf{p}}_{R_{k|k-1}}$, is employed in this computation instead of the updated estimate, $\hat{\mathbf{p}}_{R_{k|k}}$.

2. In the evaluation of the measurement Jacobian matrix $\mathbf{H}_{R_k}$ (cf. (24)) we always utilize the landmark estimate *from the first time* the landmark was detected. Thus, if a landmark was first seen at time-step ℓ, we compute the measurement Jacobian with respect to the robot pose as:

$$\mathbf{H}'_{R_k} = (\nabla \mathbf{h}_k)\mathbf{C}^T(\hat{\phi}_{R_{k|k-1}}) \begin{bmatrix}-\mathbf{I}_2 & -\mathbf{J}(\hat{\mathbf{p}}_{L_{\ell|\ell}} - \hat{\mathbf{p}}_{R_{k|k-1}})\end{bmatrix} \tag{72}$$

As a result of the above modifications, only the *first* estimates of all landmark positions and all robot poses appear in the Jacobians of the filter. This has as effect that the observability matrix $\mathbf{N}$ of this new filter, which we term *First-Estimates Jacobian* (FEJ)-EKF, assumes the form:

$$\mathbf{N}' = \begin{bmatrix} -\mathbf{I}_2 & -\mathbf{J}\left(\hat{\mathbf{p}}_{L_{\ell|\ell}} - \hat{\mathbf{p}}_{R_{k|k-1}}\right) & \mathbf{I}_2 \\ -\mathbf{I}_2 & -\mathbf{J}\left(\hat{\mathbf{p}}_{L_{\ell|\ell}} - \hat{\mathbf{p}}_{R_{k|k-1}}\right) & \mathbf{I}_2 \\ -\mathbf{I}_2 & -\mathbf{J}\left(\hat{\mathbf{p}}_{L_{\ell|\ell}} - \hat{\mathbf{p}}_{R_{k|k-1}}\right) & \mathbf{I}_2 \\ \vdots & \vdots & \vdots \\ -\mathbf{I}_2 & -\mathbf{J}\left(\hat{\mathbf{p}}_{L_{\ell|\ell}} - \hat{\mathbf{p}}_{R_{k|k-1}}\right) & \mathbf{I}_2 \end{bmatrix} \tag{73}$$

This matrix is of rank 2, and thus the FEJ-EKF is based on an error-state system model whose unobservable subspace is of dimension 3. We stress that the FEJ-EKF estimator is realizable “in the real world”, since it does not utilize any knowledge of the true state. Interestingly, even though this new filter does not use the latest available state estimates (and thus utilizes Jacobians that are less accurate than those of the standard EKF), it exhibits better consistency properties than the standard EKF. This is shown through the simulation studies of the following section.

5 Simulation Results

A series of Monte-Carlo comparison studies were conducted under various conditions, in order to validate the preceding theoretical analysis and to demonstrate the capability of the FEJ-EKF filter to improve the consistency of EKF-SLAM.

The metrics used to evaluate filter performance are: (i) the average normalized (state) estimation error squared (NEES), and (i) the root mean square (RMS) error [9]. Particularly, for the landmarks we compute the average RMS and average NEES errors by averaging the squared errors and the NEES, respectively, over all Monte Carlo runs, all landmarks and all time steps. On the other hand, for the robot pose we compute these error metrics by averaging over all Monte Carlo runs for each time step. More specifically, the NEES of the robot pose and the ith landmark at time step k are defined as:

$$\epsilon_{R_k} = \tilde{\mathbf{X}}_{R_{k|k}}^T \mathbf{P}_{R_{k|k}}^{-1} \tilde{\mathbf{X}}_{R_{k|k}} \tag{74}$$

$$\epsilon_{L_{i_k}} = \tilde{\mathbf{X}}_{L_{i_{k|k}}}^T \mathbf{P}_{L_{i_{k|k}}}^{-1} \tilde{\mathbf{X}}_{L_{i_{k|k}}} \tag{75}$$

where $\mathbf{P}_{R_{k|k}}$ and $\mathbf{P}_{L_{i_{k|k}}}$ are the submatrices of the state covariance matrix $\mathbf{P}_{k|k}$ corresponding to the robot pose and the ith landmark, respectively. Averaging over n Monte Carlo runs, we obtain the average NEES at time step k:

$$\bar{\epsilon}_{R_k} = \frac{1}{n}\sum_{j=1}^{n} \epsilon_{R_k}^{(j)} \tag{76}$$

$$\bar{\epsilon}_{L_{i_k}} = \frac{1}{n}\sum_{j=1}^{n} \epsilon_{L_{i_k}}^{(j)} \tag{77}$$

where the superscript (j) is added to denote the jth Monte Carlo run. Finally, by averaging over all time steps and over all landmarks, we obtain the average landmark NEES. Similarly, the RMS errors the robot pose and the ith landmark position from n Monte Carlo runs are defined as:

$$\xi_{R_k} = \sqrt{\frac{1}{n}\sum_{j=1}^{n} \varepsilon_{R_k}^{(j)}} \tag{78}$$

$$\xi_{L_{i_k}} = \sqrt{\frac{1}{n}\sum_{j=1}^{n} \varepsilon_{L_{i_k}}^{(j)}} \tag{79}$$

	Ideal EKF	Std. EKF	FEJ-EKF	[13]
	Position Err. RMS (m)			
Explor.	22.41	32.73	22.65	22.73
Loops	0.95	2.08	0.98	1.16
	NEES			
Explor.	2.58	6.70	2.66	4.32
Loops	2.1	12.93	2.35	6.65

Table 1: Landmark Position Estimation Performance

	Ideal EKF	Std. EKF	FEJ-EKF	[13]
	Position Err. RMS (m)			
Explor.	3.86	4.61	3.87	3.89
Loops	0.69	0.98	0.70	0.75
	Heading Err. RMS (rad)			
Explor.	0.074	0.084	0.074	0.074
Loops	0.079	0.11	0.082	0.082
	NEES			
Explor.	4.16	8.05	4.07	5.92
Loops	3.05	12.79	3.68	6.70

Table 2: Robot Pose Estimation Performance

where $\varepsilon^{(j)}_{R_k} = \tilde{\mathbf{X}}^T_{R_{k|k}} \tilde{\mathbf{X}}_{R_{k|k}}$ (or $\varepsilon^{(j)}_{L_{i_k}} = \tilde{\mathbf{X}}^T_{L_{i_{k|k}}} \tilde{\mathbf{X}}_{L_{i_{k|k}}}$) is the error norm at time step k for the jth run. Similarly, by averaging over all time steps and over all landmarks, we get the average landmark RMS.

The RMS values of the estimation errors provide us with a concise metric of the accuracy of a given estimator. On the other hand, the NEES is a powerful metric for evaluating filter consistency. Specifically, it is known that the NEES of an M-dimensional Gaussian random variable follows a χ^2 distribution with M degrees of freedom. Therefore, if a certain filter is consistent, we expect that the average NEES for the robot pose will be close to 3 for all k, and that the average landmark NEES will be close to 2. The larger the deviations of the NEES from these values, the larger the inconsistency of the filter. By studying both the RMS errors and NEES of all the filters, we obtain a comprehensive picture of the estimators' performance.

In all the simulation tests presented in this section, the robot moves at a constant velocity of $v = 0.25$ m/sec, the standard deviation of the velocity measurement noise is equal to $\sigma_v = 0.1v$, while the rotational velocity measurements are corrupted by noise with standard deviation $\sigma_\omega = 1^\circ$/sec. The robot records measurements of the relative position of landmarks that lie within its sensing range of 5 m, with standard deviation equal to 15% of the robot-to-landmark distance along each axis. 100 Monte Carlo simulations were performed, and during each run, four filters process the same data, to ensure a fair comparison. The four filters compared are: (1) the ideal EKF, (2) the standard EKF, (3) the FEJ-EKF, and (4) the robocentric filter presented in [13, 10], which aims at improving the consistency of SLAM by expressing the landmarks in a robot-relative frame. It should be pointed out that the sensor-noise levels selected for the simulations are larger than what is typically encountered in practice. This was done purposefully, since larger noise levels lead to higher estimation errors, which in turn cause the Jacobian estimates to be less accurate, and make the effects of inconsistency more apparent.

Two SLAM scenarios are considered: exploration SLAM and SLAM with loop closure. In the first case, the robot constantly explores unseen territory, without returning to already revisited areas. At the end of each run, approximately 40 landmarks have been detected. In the second case, the robot executes 10 loops on a circular trajectory, and observes 20 landmarks in total. The comparative results for all filters are presented in Figs. 1 and 2, and Tables 1 and 2. Specifically, Fig. 1(a) and Fig. 1(b) show the average NEES and RMS errors for the robot pose, respectively, for the case of exploration SLAM. Fig. 2(a) and Fig. 2(b) show the same quantities for the circular trajectory. On the other hand, Tables 1 and 2 present the average values of all relevant performance metrics for the landmarks and robot respectively, for both simulation scenarios.

Several interesting conclusions can be drawn from these results. First, it becomes clear that the performance of the FEJ-EKF is *almost identical* to that of the ideal EKF, and substantially better than the standard EKF, both in terms of RMS errors and NEES. This occurs even though the Jacobians used in the FEJ-EKF are less accurate than those used in the standard EKF, as explained in the preceding section. This fact indicates that the observability properties of the EKF error-state system model in SLAM have a more significant effect on consistency than the use of inaccurate Jacobians. Based on the Monte-Carlo results we have obtained, it appears that the errors introduced by the use of inaccurate Jacobians have a less detrimental effect on consistency than the use of an error-state system model with observable subspace of dimension larger than that of the actual, nonlinear, SLAM system.

A second observation is that the FEJ-EKF also performs better than robocentric mapping [13], both in terms of accuracy and in terms of consistency. One possible justification for this is based on the fact that in robocentric mapping, during each propagation step *all* landmark position estimates need to be changed, since they are expressed with respect to the moving robot frame. As a result, during each propagation step (termed *composition* in [13]), all landmark estimates and their covariance are affected by the linearization errors of the process model. This problem does not exist in the world-centric formulation of SLAM, and it could offer an explanation for the observed behavior. As a final remark, we note that even though the FEJ-EKF NESS performance is significantly better compared to that of the robocentric mapping, the difference in the RMS errors of the two filters is less pronounced. This indicates that the effects of inconsistency primary affect the *covariance*, rather than the *state* estimates.

6 Conclusions

In this paper, we have studied in depth the issue of filter inconsistency in EKF-based SLAM, from an observability perspective. By comparing the observability properties of the nonlinear SLAM system model with those of the linearized error-state model employed in the EKF, we proved that the observable subspace of the standard EKF is always of higher dimension than the observable subspace of the underlying nonlinear system. As a result, the covariance estimates of the EKF undergo reduction in directions of the state space where no information is available, which is a primary cause of inconsistency. Based on the above analysis, a new "First Estimates Jacobian" (FEJ) EKF is proposed to improve the estimator's consistency during SLAM. The proposed algorithm performs better with respect to consistency, because when the filter Jacobians are calculated using the first available estimate for each state variable, the error-state system model has an observable subspace of the same dimension as the underlying nonlinear SLAM system. Through extensive Monte-Carlo simulations we have verified that the FEJ-EKF is more accurate and more consistent than both the standard EKF and robocentric mapping [13], which has been proposed for improving estimator consistency in SLAM.

References

[1] R. Smith and P. Cheeseman. On the representation and estimation of spatial uncertainty. *International Journal of Robotics Research*, 5(4):56–68, 1987.

[2] M. Montemerlo. *FastSLAM: A factored solution to the simultaneous localization and mapping problem with unknown data association.* PhD thesis, Carnegie Mellon University, 2003.

[3] M. Paskin. *Thin Junction Tree Filters for Simultaneous Localization and Mapping.* PhD thesis, UC Berkeley, 2002.

[4] J. Neira and J. Tardos. Data association in stochastic mapping using the joint compatibility test. *IEEE Transactions on Robotics and Automation*, 17(6):890 – 897, 2001.

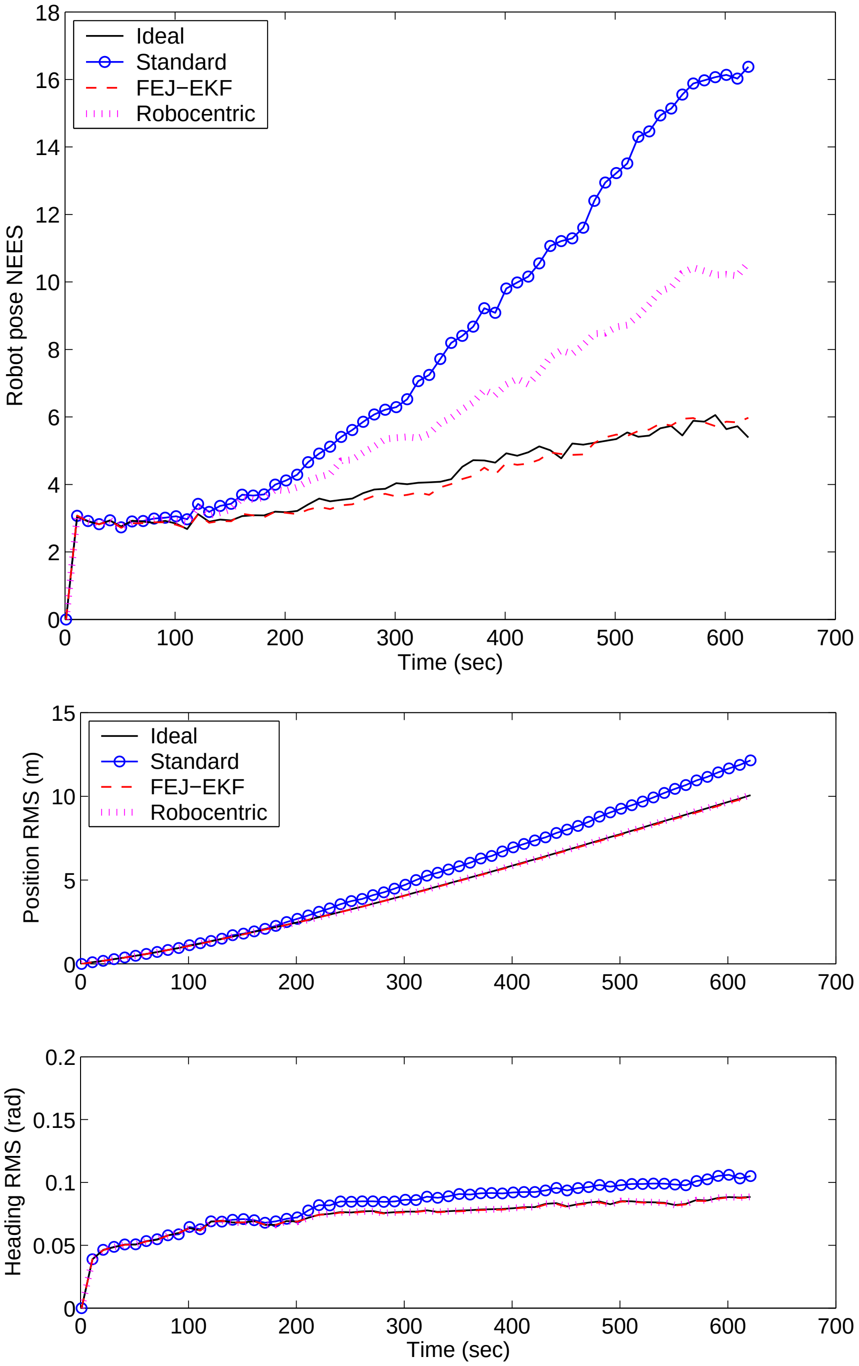

Figure 1: Monte Carlo results for an exploration-SLAM scenario. (a) Average NEES of the robot pose errors (b) RMS errors for the robot pose (position and orientation). In these plots, the solid lines correspond to the ideal EKF, the dashed lines to the FEJ-EKF, the solid lines with circles to the standard EKF, and the dotted lines to the robocentric mapping algorithm of [13]. Note that the RMS errors of the ideal EKF, the FEJ-EKF, and the robo-centric SLAM algorithm are almost identical, which makes the corresponding lines difficult to distinguish.

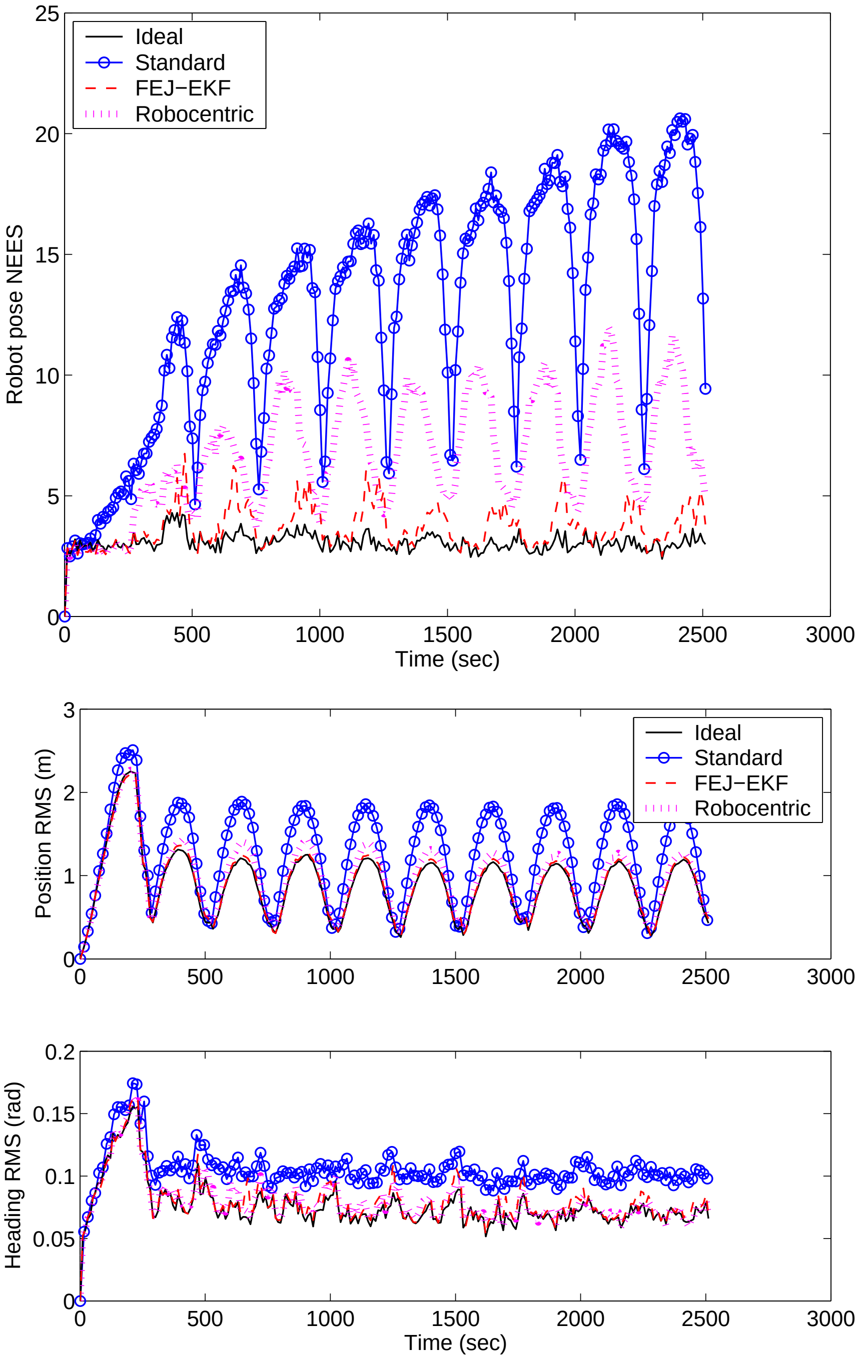

Figure 2: Monte Carlo results for a SLAM scenario with multiple loop closures. (a) Average NEES of the robot pose errors (b) RMS errors for the robot pose (position and orientation). In these plots, the solid lines correspond to the ideal EKF, the dashed lines to the FEJ-EKF, the solid lines with circles to the standard EKF, and the dotted lines to the robocentric mapping algorithm of [13]. Note that the RMS errors of the ideal EKF and the FEJ-EKF SLAM algorithm are almost identical, which makes the corresponding lines difficult to distinguish.

[5] S. Se, D. Lowe, and J. Little. Mobile robot localization and mapping with uncertainty using scale-invariant visual landmarks. *International Journal of Robotics Research*, 21(8):735 – 758, 2002.

[6] P. Newman. *On the structure and solution of the simultaneous localization and mapping problem.* PhD thesis, University of Sydney, 1999.

[7] S. B. Williams, P. Newman, M. Dissanayake, and H. Durrant-Whyte. Autonomous underwater simultaneous localisation and map building. In *IEEE International Conference on Robotics and Automation (ICRA)*, pages 1793–1798, San Francisco, CA, April 2000.

[8] J. H. Kim and S. Sukkarieh. Airborne simultaneous localisation and map building. In *IEEE International Conference on Robotics and Automation (ICRA)*, pages 406–411, Taipei, Taiwan, September 2003.

[9] Y. Bar-Shalom, X. R. Li, and T. Kirubarajan. *Estimation with applications to tracking and navigation.* New York: Wiley, 2001.

[10] J.A. Castellanos, R. Martinez-Cantin, J. Tardos, and J. Neira. Robocentric map joining: Improving the consistency of EKF-SLAM. *Robotics and Autonomous Systems*, 55:21–29, 2007.

[11] T. Bailey, J. Nieto, J. Guivant, M. Stevens, and E. Nebot. Consistency of the EKF-SLAM algorithm. In *IEEE/RSJ International Conference on Intelligent Robots and Systems (IROS)*, pages 3562–3568, Beijing, China, October 2006.

[12] S. Julier and J. Uhlmann. A counter example to the theory of simultaneous localization and map building. In *IEEE International Conference on Robotics and Automation (ICRA)*, pages 4238–4243, 2001.

[13] J.A. Castellanos, J. Neira, and J. Tardos. Limits to the consistency of EKF-based SLAM. In *5th IFAC Symposium on Intelligent Autonomous Vehicles*, Lisbon, Portugal, July 2004.

[14] S. Huang and G. Dissanayake. Convergence analysis for extended Kalman filter based slam. In *IEEE Conference on Robotics and Automation (ICRA)*, pages 412–417, Orlando, Florida, May 2006.

[15] J. Andrade-Cetto and A. Sanfeliu. The effects of partial observability in SLAM. In *IEEE International Conference on Robotics and Automation (ICRA)*, pages 394–402, New Orleans, LA, April 2004.

[16] J. Andrade-Cetto and A. Sanfeliu. The effects of partial observability when building fully correlated maps. *IEEE Transactions on Robotics*, 21(4):771–777, 2005.

[17] K. W. Lee, W. S. Wijesoma, and J. I. Guzman. On the observability and observability analysis of SLAM. In *IEEE/RSJ Intenational Conference on Intelligent Robots and Systems (IROS)*, pages 3569–3574, Beijing, China, October 2006.

[18] R. Hermann and A. Krener. Nonlinear controllability and observability. *IEEE Transactions on Automatic Control*, 22:728 – 740, 1977.

[19] Z. Chen, K. Jiang, and J. C. Hung. Local observability matrix and its application to observability analyses. In *16th Annual Conference of IEEE (IECON'90)*, pages 100–103, Pacific Grove, CA, USA, November 1990.